Supplementary Information

Structural and mechanistic insights into the constitutive Themis–Grb2 complex in T cell signalling

Danielle M. Clancy*, Alba Sanz-Sanjuan, Elisabeth Gilis, Peter Tougaard, Imke Velghe, Yana Van Droogenbroeck, Jan Felix, Yehudi Bloch, Álvaro Furones Cuadrado, Romain Merceron, Stephan Schenck, Peter Vandenabeele, Janine D. Brunner, Tom Taghon, Dirk Elewaut, Savvas N. Savvides*

*Correspondence: danielle.clancy@irc.vib-ugent.be ; savvas.savvides@ugent.be

SUPPLEMENTARY FIGURES

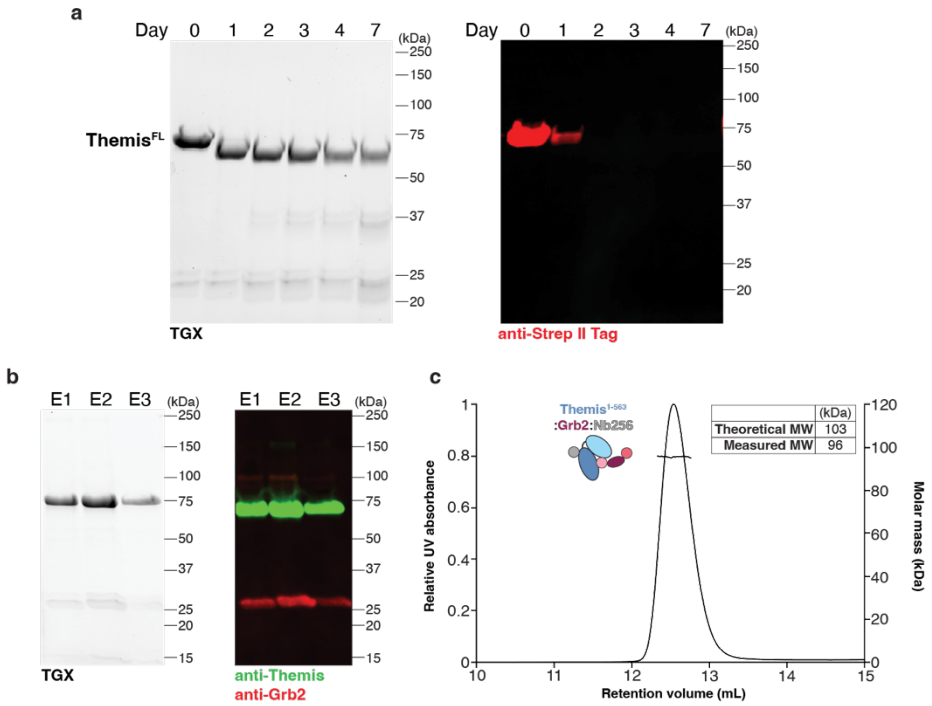

Supplementary Figure 1. Recombinant Themis co-purifies with endogenous Grb2

a, Full-length C-terminal StrepII-tagged Themis (Themis^{FL}) was expressed and purified from HEK suspension cells. Purified recombinant Themis^{FL} was incubated at room temperature and samples were taken at indicated timepoints to check protein stability. Representative TGX gel and western blot analysis with an anti-StrepII tag antibody is shown. The predominant band at approximately 73 kDa corresponds to purified Themis^{FL}. Themis^{FL} loses its C-terminal StrepII tag and moves to a lower molecular weight (MW) over time. **b,** Themis was expressed and purified from HEK suspension cells. Representative TGX gel analysis of elution (E) fractions after affinity purification. The same gel was probed with specific anti-Themis and anti-Grb2 antibodies and detected with fluorescently tagged secondary antibodies. A fraction of endogenous cellular Grb2 was pulled down during Themis^{FL} purification from HEK suspension cells. **c,** SEC-MALLS analysis of co-expressed and purified Themis$^{1-563}$-Grb2 in complex with Nb256. The Themis$^{1-563}$-Grb2-Nb256 complex has a theoretical mass of 103 kDa. Data are representative of two independent experiments.

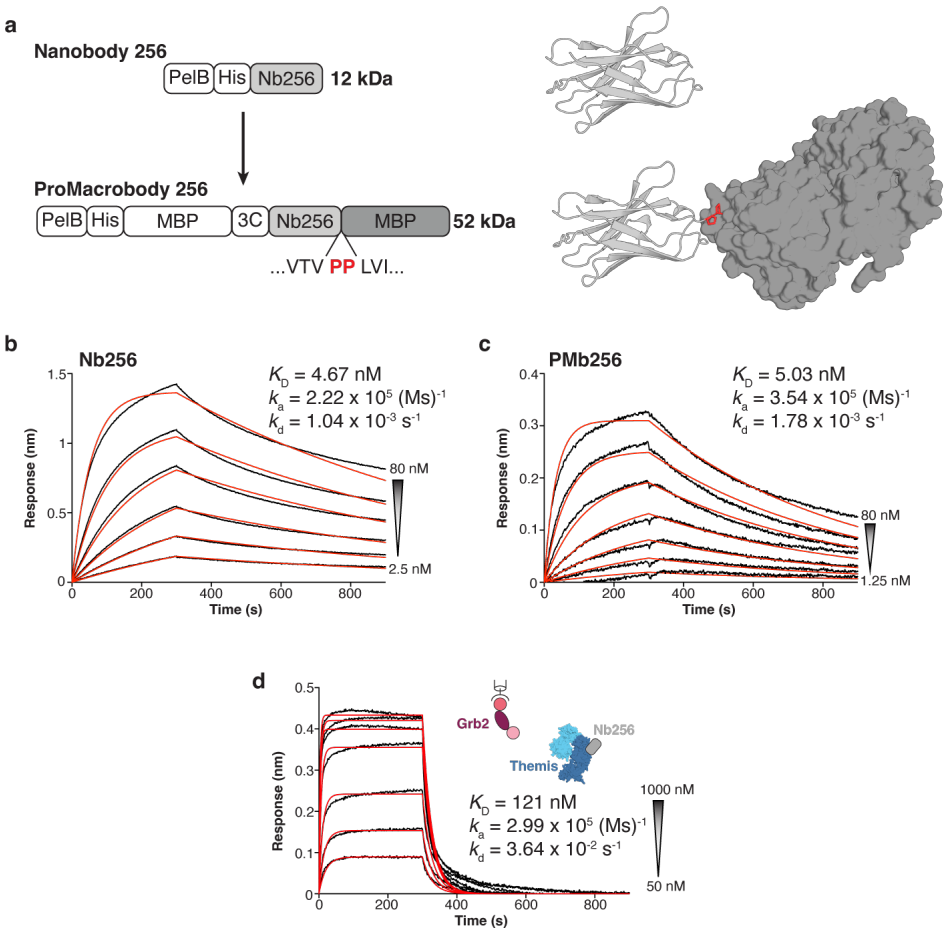

Supplementary Figure 2. Conversion of Nb256 to PMb256

a, Comparison of the construct layout for the expression of Nb256 and PMb256. The original Nb construct contained a pelB leader sequence for periplasmic expression, followed by a hexahistidine (His6) tag and the Nb256 sequence. To generate PMb256, the Nb256 sequence was cloned into a pBXNPH3M expression vector containing a PelB leader sequence, followed by a decahistidine (His10) tag, MBP and 3C protease site. A truncated MBP moiety starting at residue Leu7 (LVI…) is encoded C-terminal to the Nb256 sequence, connected by a rigid double proline linker. Cartoon representations of Nb256 and PMb256 are shown. Structures were extracted from the cryo-EM model of the Themis$^{1\text{-}563}$-Grb2-PMb256 complex. The double proline linker is coloured in red and the MBP moiety is shown in surface representation. **b,** Representative BLI response curve to characterize binding of Themis$^{1\text{-}563}$ to immobilized Nb256. Data are representative of three independent experiments. **c,** Representative BLI response curve to characterize binding of Themis1-563 to immobilized PMb256. **d,** Representative BLI response curve for the interaction of immobilized Grb2^{FL} with Themis$^{1\text{-}563}$ in complex with Nb256. Response curves were fitted with a 1:1 model (red) to quantify the kinetics (k_a, k_d) and binding affinity (K_D). Start and end concentrations of the 2-fold dilution series of the analyte is shown as an inset. Data are representative of two independent experiments.

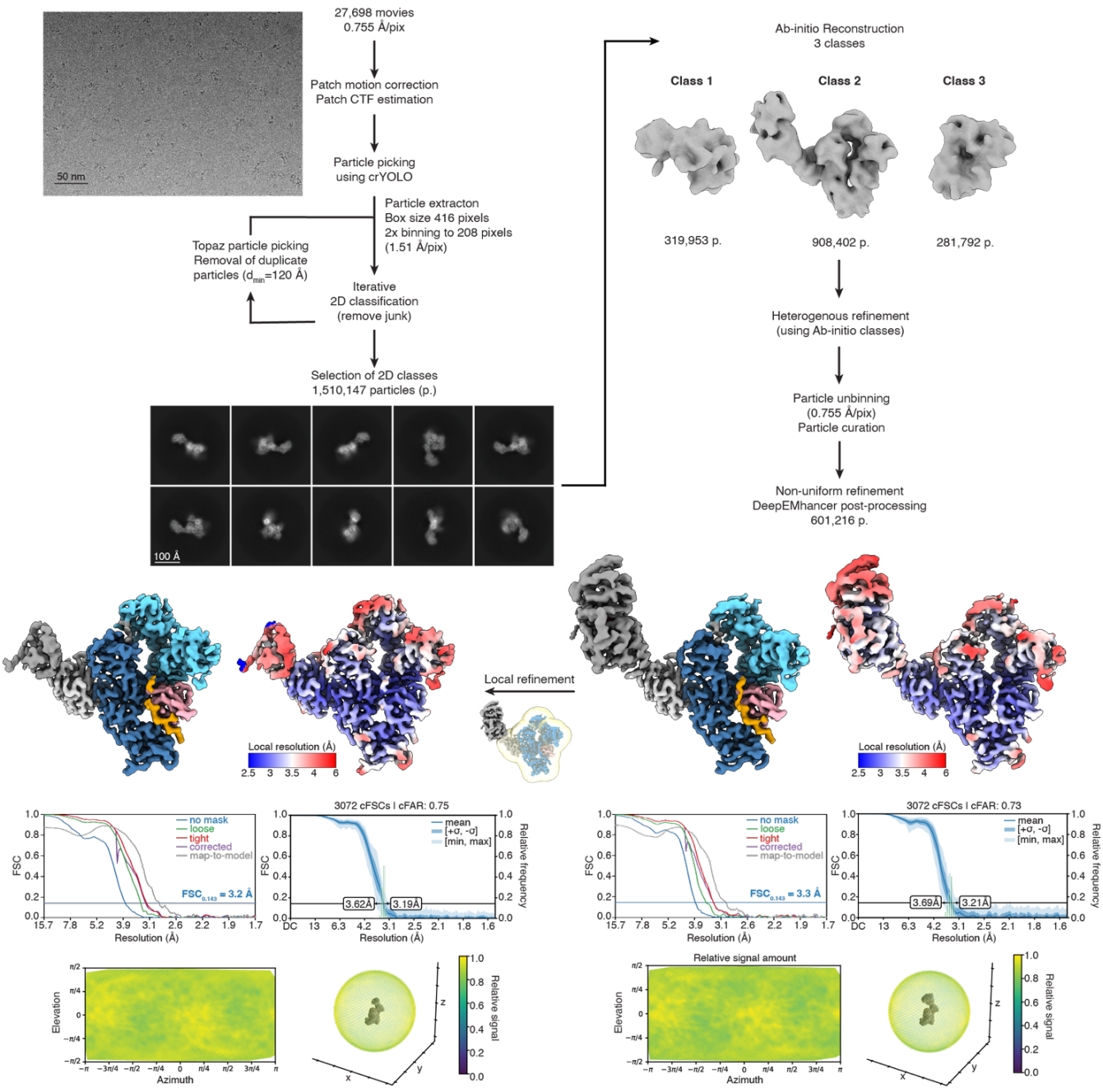

Supplementary Figure 3. Cryo-EM data processing workflow for the Themis$^{1\text{-}563}$-Grb2-PMb256 complex

Data processing was performed in CryoSPARC v4.5.1[47,48] and map post-processing was performed using DeepEMhancer[53]. Gold standard Fourier Shell Correlation (FSC) curves are shown and the estimated resolution at FSC = 0.143 (blue line) is shown for the corrected FSC curves (purple line).

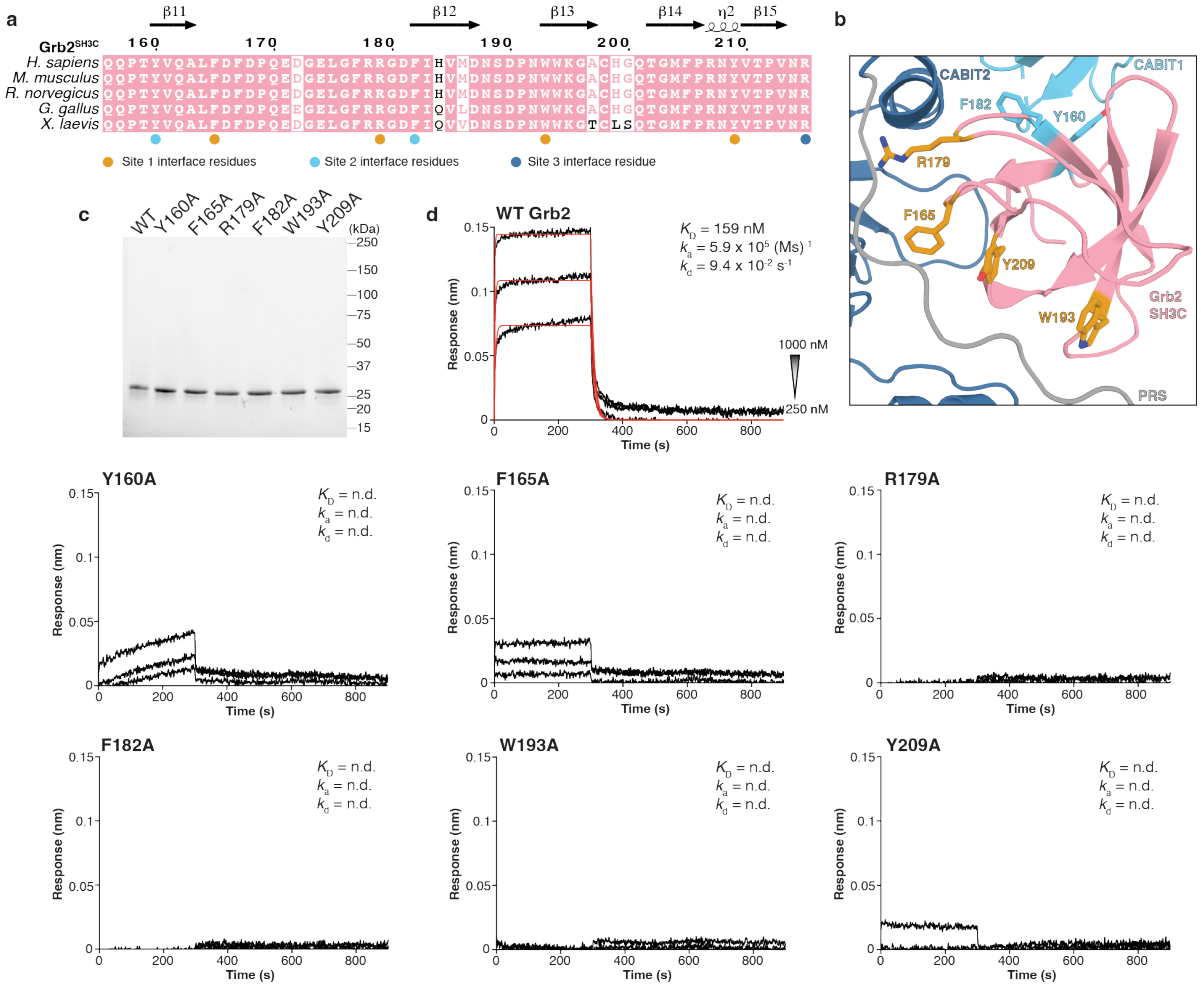

Supplementary Figure 4. Functional interrogation of Grb2^{SH3C} mutants

a, Sequence alignment of various vertebrate Grb2^{SH3C} sequences using the ESPripT server (https://espript.ibcp.fr) and structural annotation according to secondary structure elements. Coloured symbols indicate residues participating in interaction sites 1-3. *H. sapiens* (Homo sapiens); *M. musculus* (Mus musculus); *R. norvegicus* (Rattus norvegius); *G. gallus* (Gallus gallus); *X. laevis* (Xenopus laevis). **b,** Zoom-in view of the Themis$^{1-563}$-Grb2^{SH3C} interaction interfaces. Site 1 and site 2 interface residues targeted by mutagenesis are shown in stick representation and coloured as in **a**. Grb2^{SH3C}, Themis^{PRS}, Themis^{CABIT1}, Themis^{CABIT2} are shown in pink, orange, cyan and dark blue, respectively. **c,** Representative SDS-PAGE analysis of purified Grb2^{SH3C} mutants used in BLI experiments. All mutant variants displayed similar biochemical behaviour to wild-type (WT) Grb2 **d,** BLI response curves for the interaction of immobilized WT or mutant Grb2FL variants with Themis$^{1-563}$. A 1:1 binding model was fitted (in red) to quantify the kinetics (k_a, k_d) and binding affinity (K_D). Start and end concentrations of the 2-fold dilution series of the analyte is shown as an inset. For all Grb2 mutants tested, kinetics and affinity could not be determined (n.d.) due to no binding or poor data fitting. Data are representative of at least two independent experiments.

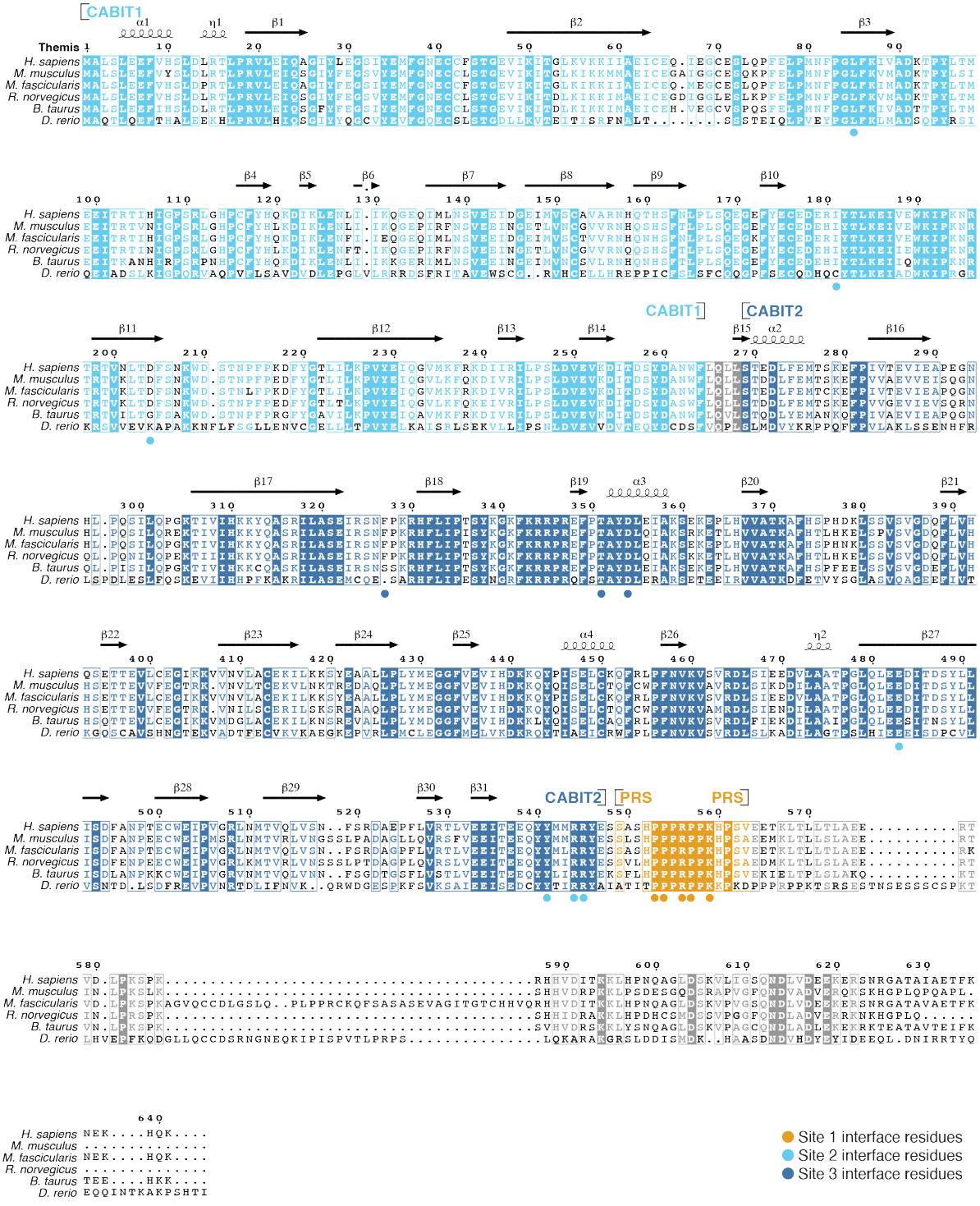

Supplementary Figure 5. Conservation of Grb2^{SH3C} interfacing residues in Themis

Structurally annotated multiple sequence alignment of various vertebrate Themis sequences using the ESPripT server (https://espript.ibcp.fr). Coloured symbols indicate residues participating in interaction sites 1-3. CABIT1, CABIT2 and PRS domain delineations are indicated. *H. sapiens* (Homo sapiens); *M. musculus* (Mus musculus); *M. fascicularis* (Macaca fascicularis); *R. norvegicus* (Rattus norvegius); *B. taurus* (Bos taurus); *D. rerio* (Danio rerio).

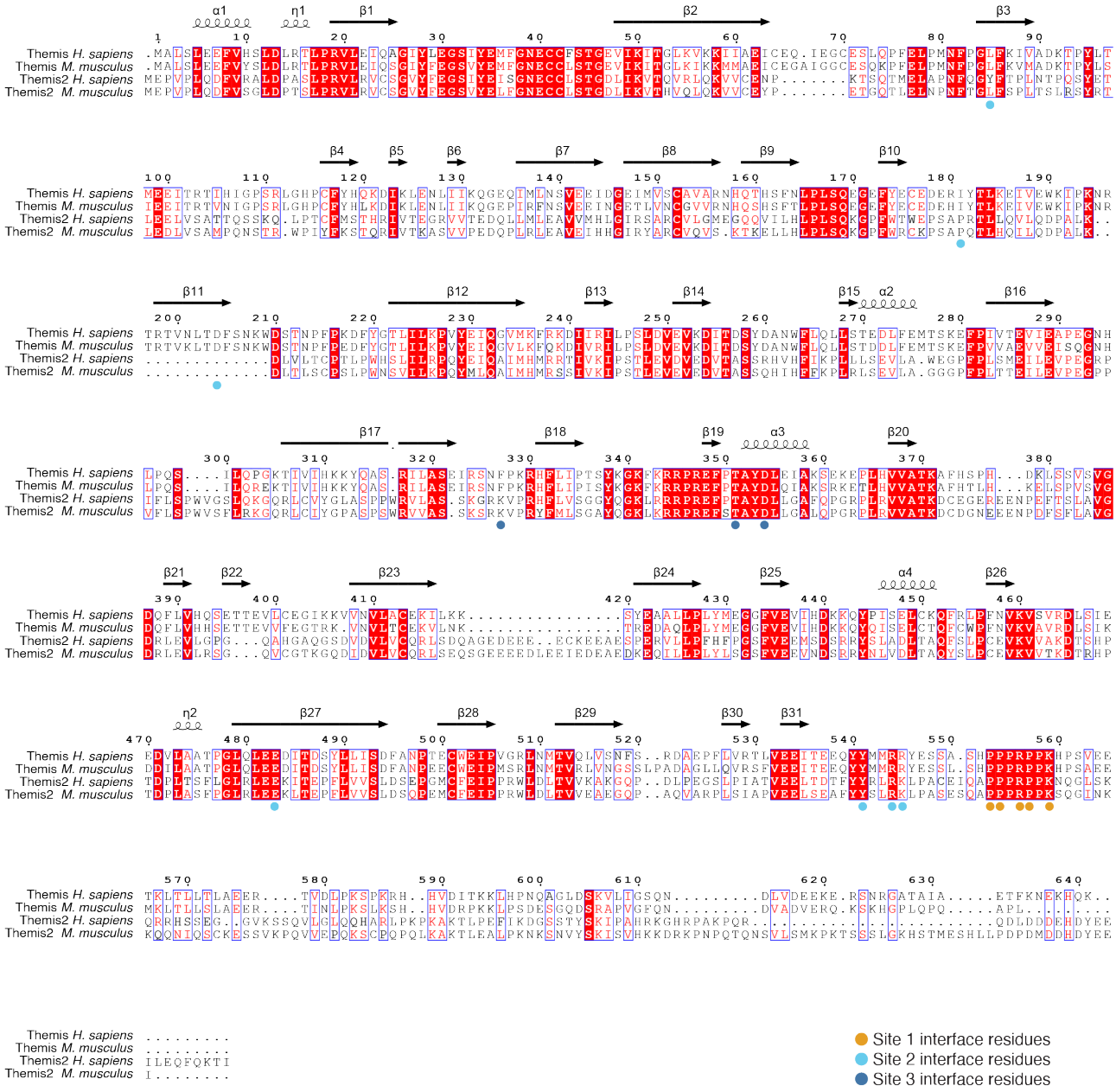

Supplementary Figure 6. Sequence alignment of Themis and Themis2

Structurally annotated multiple sequence alignment of Themis and Themis2 sequences using the ESPripT server (https://espript.ibcp.fr). Coloured symbols indicate residues participating in interaction sites 1-3 with Grb2SH3C. *H. sapiens* (Homo sapiens); *M. musculus* (Mus musculus).

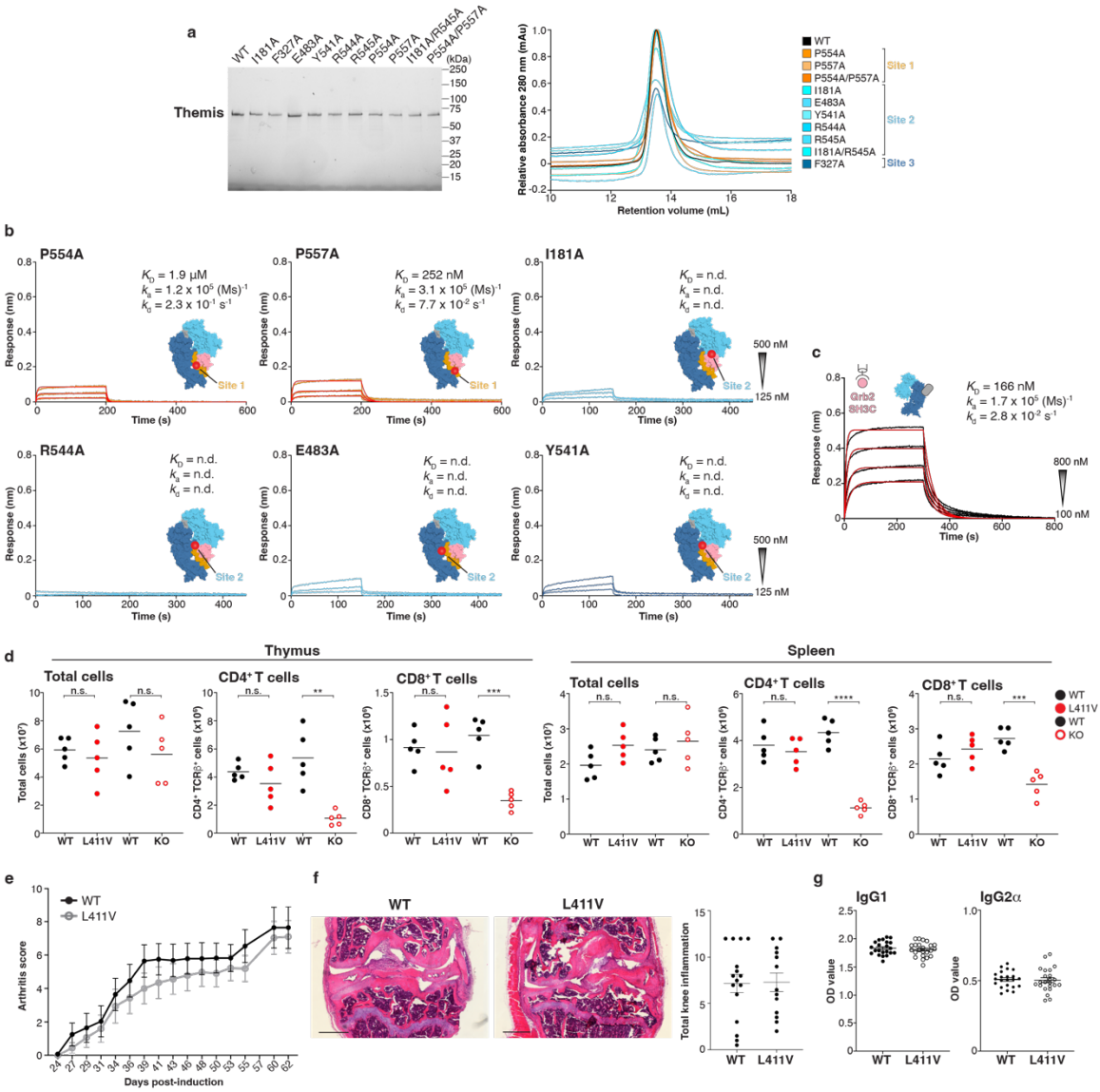

Supplementary Figure 7. Functional interrogation of Themis mutants

a, SDS-PAGE analysis and representative SEC chromatograms of purified Themis$^{1\text{-}563}$ mutants. All mutant variants displayed similar biochemical behaviour to wild-type (WT) Themis$^{1\text{-}563}$. Data are representative of two independent purifications. **b,** BLI response curves for the interaction of immobilized WT Grb2^{FL} with Themis$^{1\text{-}563}$ mutants. A 1:1 binding model was fitted (in red) to quantify the kinetics (k_a, k_d) and binding affinity (K_D). Kinetics and affinity could not be determined (n.d.) for the indicated mutants due to no binding or poor data fitting. The location of each mutation in the Themis$^{1\text{-}563}$-Grb2^{SH3C} interface are indicated on a surface representation of the complex. Data are representative of two experiments. **c,** BLI response curve for the interaction of immobilized GST-Grb2^{SH3C} with Themis$^{1\text{-}563}$ in complex with Nb256. A 1:1 binding model was fitted (in red) to quantify the kinetics (k_a, k_d) and binding affinity (K_D). For all BLI experiments, start and end concentrations of the 2-fold dilution series is shown as an inset. **d,** Total cellularity and quantification of CD4$^+$ and CD8$^+$ single positive T cell populations in the thymus and spleen of Themis^{KO} and Themis^{L411V} mice compared to wild-type (WT) littermates by flow cytometry. Data are from one experiment with five mice per group. Bars represent the mean of the data. n.s. non-significant, **p = 0.00144, ***p = 0.00012, (Thymus) and ***p = 000264, ****p = 0.000003 (Spleen) by two-tailed t-test. **e,** Clinical arthritis scores were assessed in the ankle joints of mice after induction of CIA, in groups of male Themis^{L411V} transgenic mice (n=23) and wild-type (WT) littermates (n=23). Results are the mean ± SEM. **f,** Knee joints of male WT or Themis^{L411V} transgenic mice were examined for histological features of arthritis to confirm the clinical data. Hematoxylin and eosin staining was carried out to assess the amount of infiltrate and exudate in the femorotibial joints. Scale bars represent 500 µm. **g,** Serum antibody levels of IgG1 and IgG2α anti-collagen antibodies from WT and Themis^{L411V} mice were measured by ELISA. Bars represent the mean of the data.

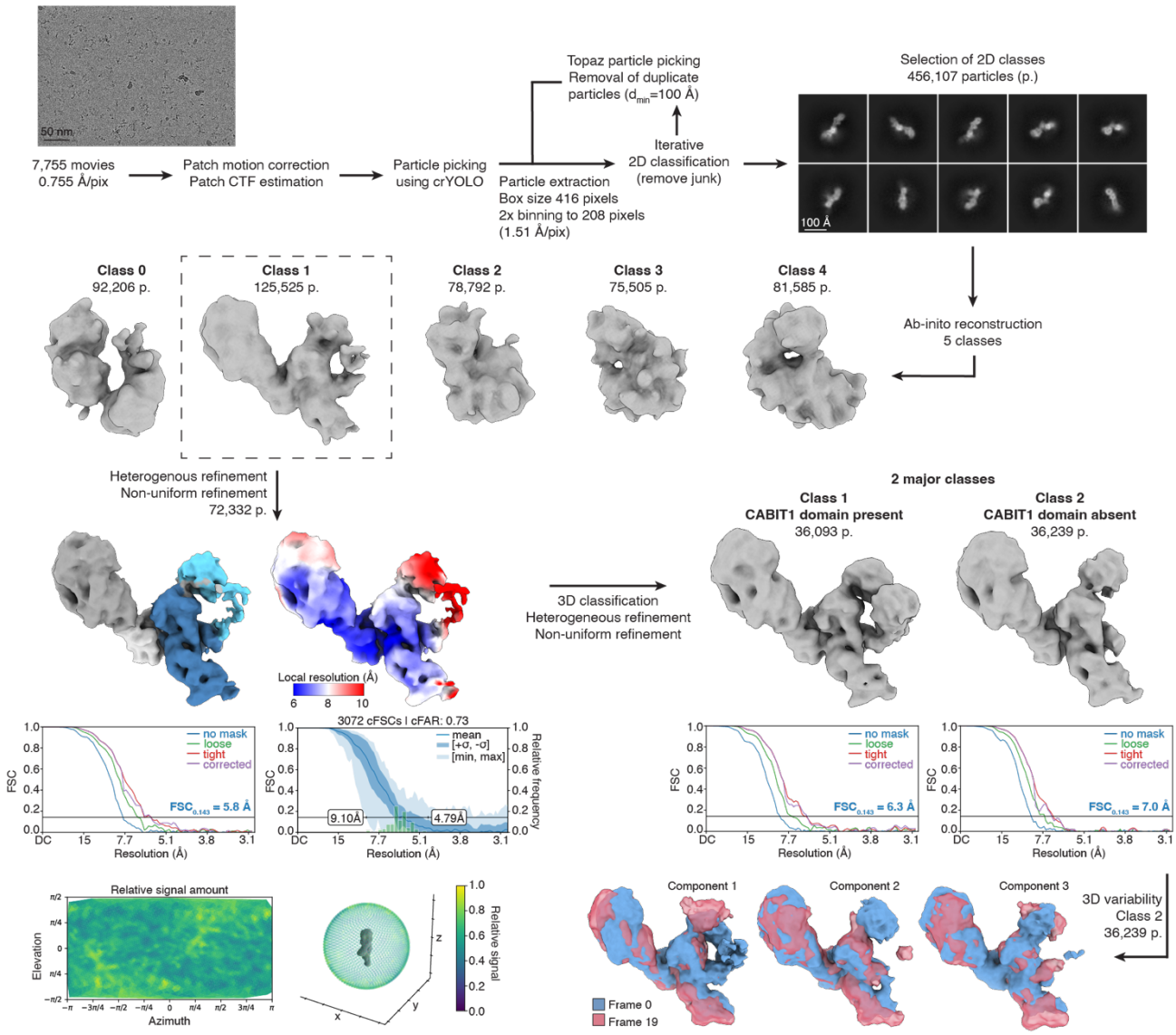

Supplementary Figure 8. Cryo-EM data processing workflow for the Themis$^{1\text{-}563}$-PMb256 complex

Data processing was performed in CryoSPARC v4.5.1. Sharpened maps from non-uniform refinement in CryoSPARC are shown. Gold standard Fourier Shell Correlation (FSC) curves are shown and the estimated resolution at FSC = 0.143 (blue line) is shown for the corrected FSC curves (purple line).

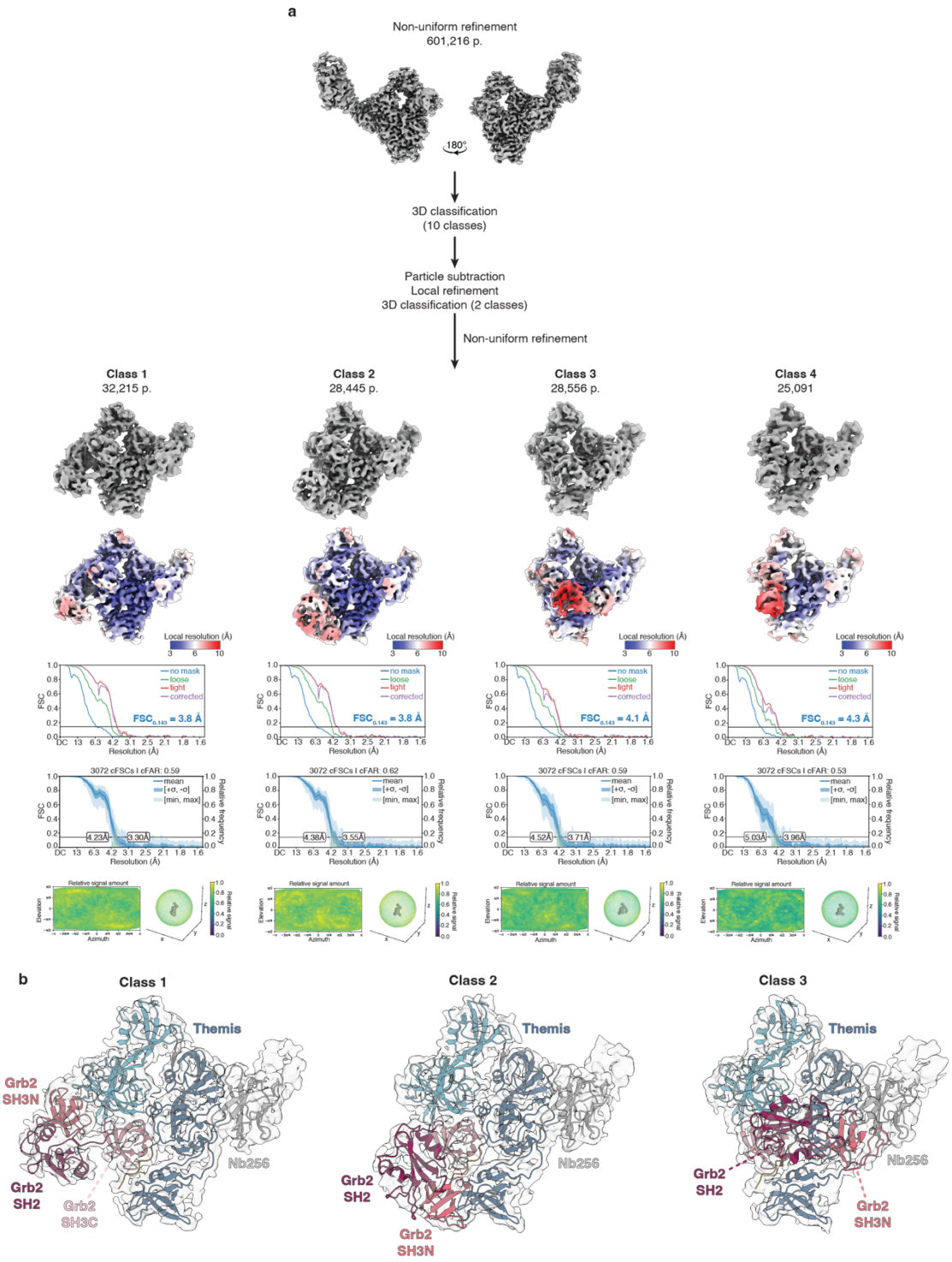

Supplementary Figure 9. 3D classification and data processing workflow to identify conformational heterogeneity of Grb2^{SH3N} and Grb2^{SH2} domains

a, Particles (601,216 p.) contributing to the Themis$^{1-563}$-Grb2-PMb256 map were further analysed in a 3D classification job without alignment. The resulting 4 classes exhibiting volume corresponding to the N-terminal domains of Grb2 were subjected to particle subtraction to remove the MBP moiety from the PMb followed by local refinement. Final particle numbers (p.) and sharpened maps from non-uniform refinement for each class are shown. Gold standard Fourier Shell Correlation (FSC) curves are shown and the estimated resolution at FSC = 0.143 (blue line) is shown for the corrected FSC curves (purple line). Data processing was performed in CryoSPARC v4.5.1. **b**, Rigid body fitting of Grb2^{SH3N} and Grb2^{SH2} domains in cryo-EM maps from Class 1-3 identified from 3D classification in **a**. Models of individual Grb2^{SH3N} and Grb2^{SH2} domains were predicted using AlphaFold3 and independently rigid body fitted in sharpened maps in ChimeraX. The flexible loops between the SH3N and SH2 domans were subsequently connected and adjusted using local real-space refinement in Coot, specifically restricted to the connecting loop regions supported by density.

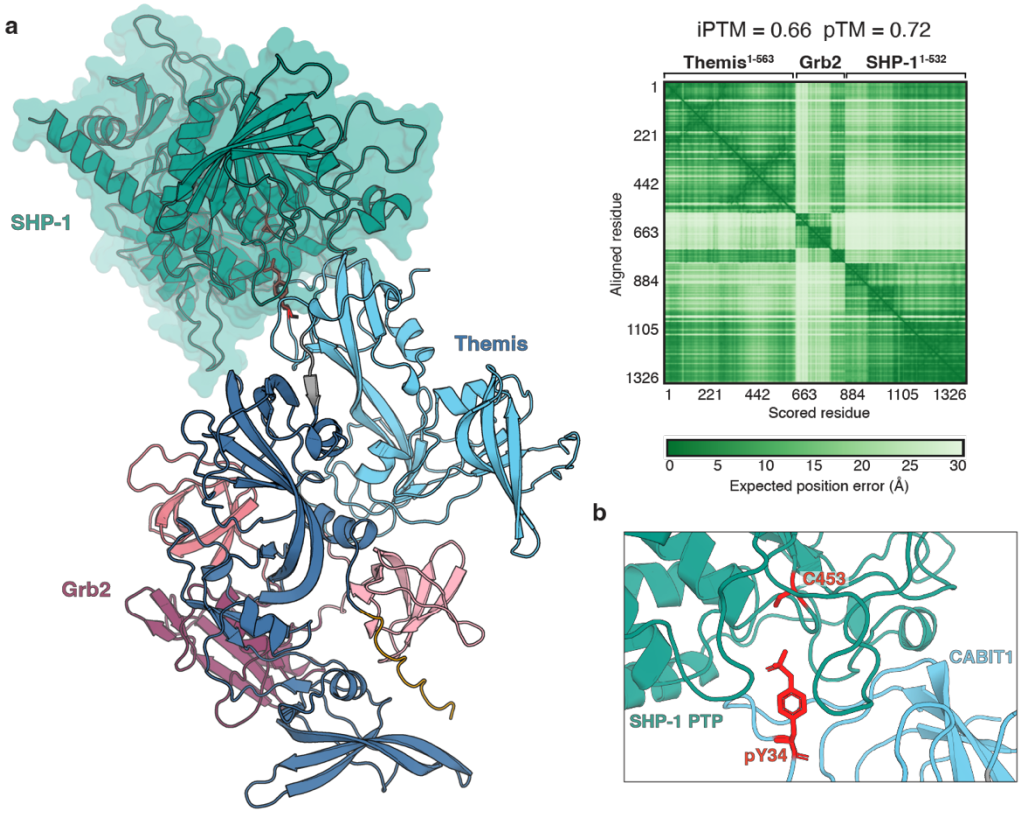

Supplementary Figure 10. AlphaFold3 predicts the formation of a Themis-Grb-SHP-1 ternary complex

a, AlphaFold3 prediction of Themis$^{1-563}$ in complex with Grb2^{FL} and SHP-1$^{1-532}$ using the Google Deepmind webserver (https://golgi.sandbox.google.com). Phosphorylation of Tyr34 (pY34) in Themis was included as a post-translational modification in the prediction of the complex. Truncated sequences for Themis and SHP-1 were used for prediction to exclude lower confidence scores caused by intrinsically disordered sequences at the C-termini of these proteins. Truncated SHP-1 lacking the flexible 61 residue C-terminal tail (residues 1-532) has previously been characterized using X-ray crystallography. Themis and Grb2^{FL} are coloured as before. SHP-1 is coloured in teal and depicted as a surface representation overlaying the cartoon representation. The iPTM and PTM scores and PAE plot are included as confidence metrics. **b,** Zoom-in view of the predicted interface between Themis pY34 and the catalytic pocket of SHP-1 phosphatase (PTP) domain. Themis pY34 and the active site cysteine of SHP-1 (C453) are depicted in stick representation and coloured red.

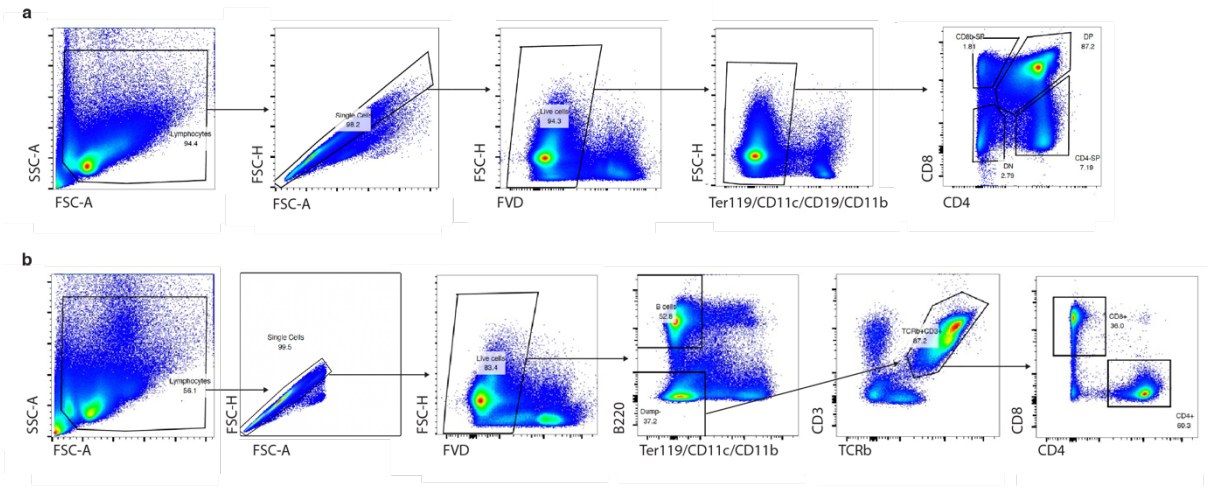

Supplementary Figure 11. Gating strategies for immunophenotyping by flow cytometry

Flow cytometry gating strategy for immunophenotyping of $CD4^+$ and $CD8^+$ cells from the **a,** thymus and **b,** spleen of WT, $Themis^{KO}$ and $Themis^{L411V}$ mice for immunophenotyping. Lymphocytes were identified using forward and side scatter. From this lymphocyte gate, single cells and live cells (using fixable viability dye (FVD)) were sequentially selected. Erythrocytes (Ter119), dendritic cells (CD11c), myeloid cells (CD11b) and B cells (CD19/B220) were gated out before gating for $CD4^+$ and $CD8^+$ cells.

SUPPLEMENTARY TABLES

Supplementary Table 1. Analysis of Themis$^{1-563}$-Grb2-PMb256 interaction interfaces

Interacting residues in the Themis$^{1-563}$-Grb2^{SH3C} and Themis$^{1-563}$-PMb256 interfaces as determined by the PISA server (https://www.ebi.ac.uk/pdbe/pisa/) and manual validation.

Themis$^{1-563}$-Grb2		
Themis$^{1-563}$	Grb2^{SH3C}	Distance (Å)
Hydrogen bonds		
ARG 556 [NH1]	GLU 174 [OE1]	3.07
ARG 111 [NH1]	ARG 179 [O]	3.60
ARG 111 [NH2]	ARG 179 [O]	3.74
ARG 111 [NH2]	ASP 181 [OD1]	3.59
ARG 180 [NH2]	ASP 181 [OD1]	3.05
TYR 541 [O]	GLN 162 [NE2]	3.09
GLU 547 [OE2]	ARG 179 [NH1]	2.96
GLU 483 [OE1]	ARG 179 [NH2]	2.75
PRO 557 [O]	TRP 193 [NE1]	3.56
PRO 558 [O]	TRP 193 [NE2]	3.58
ASP 354 [OD2]	ARG 207 [NH2]	2.45
TYR 353 [OH]	ASN 208 [ND2]	3.64
PRO 554 [O]	TYR 209 [OH]	3.13
TYR 541 [OH]	ASN 214 [N]	3.52
ASP 204 [OD1]	ARG 215 [NH2]	2.59
PHE 205 [O]	ARG 215 [NH2]	3.70
SER 325 [O]	ASN 216 [ND2]	3.55
Salt bridges		
LYS 559 [NZ]	GLU 171 [OE1]	3.44
ARG 556 [NH1]	GLU 174 [OE1]	3.07
ARG 556 [NH1]	GLU 174 [OE2]	3.65
ARG 111 [NH2]	ASP 181 [OD1]	3.59
ARG 180 [NH2]	ASP 181 [OD1]	3.05
GLU 547 [OE2]	ARG 179 [NH1]	2.96
GLU 547 [OE2]	ARG 179 [NH2]	3.68
GLU 483 [OE1]	ARG 179 [NH2]	2.75
ASP 354 [OD2]	ARG 207 [NH1]	3.53
ASP 354 [OD1]	ARG 207 [NH2]	3.63
ASP 354 [OD2]	ARG 207 [NH2]	2.45
ASP 204 [OD2]	ARG 215 [NH2]	3.48
ASP 204 [OD1]	ARG 215 [NH2]	2.59
Buried residues (numerical order)		
LEU 85	TYR 160	
ILE 181	PHE 165	
PHE 327	PHE 182	
THR 351		
ARG 544		
ARG 545		
PRO 553		

Themis$^{1-563}$-PMb256		
Themis$^{1-563}$	PMb256	Distance (Å)
Hydrogen bonds		
SER 462 [O]	TYR 32 [OH]	3.88
GLU 469 [O]	TYR 105 [N]	2.81
LEU 466 [O]	TYR 105 [OH]	3.50
GLU 469 [OE2]	TRP 108 [NE1]	3.72
ARG 464 [NH1]	ASP 99 [OD2]	2.52
ASP 471 [N]	VAL 103 [O]	3.24
Salt bridges		
GLU 469 [OE1]	ARG 45 [NH2]	3.94
GLU 470 [OE1]	ARG 104 [NH1]	3.99
ARG 464 [NH1]	ASP 99 [OD2]	2.52
Buried residues (numerical order)		
VAL 463	PHE 37	
ALA 474	LYS 43	
ASN 497	GLU 44	
LEU 527		

Supplementary Table 2. sgRNA for CRISPR-mediated Themis knockout *in vitro*

Themis-specific sgRNAs were designed using CHOPCHOP for deletion of Themis *in vitro*. The sgRNAs used were as follows:

Oligo #1	5'- CACCG GGATGACAGCTTGTCATGAG – 3'
Oligo #2	5'- AAAC CTCATGACAAGCTGTCATCC C – 3'

Supplementary Table 3. Antibodies for immunophenotyping by flow cytometry

Antibody clones and dilutions used for immunophenotyping by flow cytometry.

Antigen	Fluorochrome	Clone	Source	Catalog no.	Dilution
CD117	BB515	2B8	BD Biosciences	564481	1:100
CD44	BV421	IM7	BD Horizon	560451	1:400
CD8β	BV510	YTS156.7.7	Biolegend	126631	1:400
CD25	BV605	PC61	BD Horizon	563061	1:200
TCRβ	BV711	H57-597	BD Horizon	563135	1:100
CD11c	BV785	N418	Biolegend	117336	1:400
CD19	BV785	B4	Biolegend	115543	1:200
CD11b	BV785	M1/70	Biolegend	101243	1:400
CD4	AF647	GK1.5	Biolegend	100424	1:400
CD62L	FITC	MEL-14	Thermo Fisher	11-0621-82	1:400
NK1.1	PE-Cy7	PK136	BD Pharmingen	552878	1:100
CD3	BUV395	145-2C11	BD Horizon	563565	1:50
CD24	BUV737	M1/69	BD Horizon	565308	1:200
CD27	BUV737	LG.3A10	BD Horizon	565307	1:200